Supervisory controller for minimizing fuel consumption and NOx emissions of plug-in hybrid electric vehicles operating in zero-emission zones

Douglas Uberti Pinto[1], Benjamín Pla[1], André Nakaema Aronis[1], Emmanuele Frasci[2] and Ivan Arsie[2]

Abstract

This paper introduces a supervisory controller designed for Plug-in Hybrid Electric Vehicles (PHEVs) to minimize total energy consumption and tailpipe NOx emissions while adhering to Zero Emission Zone (ZEZ) constraints. The case study exploits historical driving cycle data from an urban bus route in Zurich to analyze trip correlations, where a ZEZ restriction was added to assess the vehicle performance under such conditions. A PHEV bus model was built, integrating the powertrain and After-Treatment System (ATS), where an electric heater is included to mitigate NOx emissions. The supervisory controller is tasked with determining the optimal power split and the electric heater power to ensure adherence to feasible operating conditions along the route. Historical driving cycle data analysis demonstrates that the speed profiles along the selected route exhibit similarities. This observation is leveraged by a Dynamic Programming (DP) optimization, where an arbitrary bus trip is employed to generate a cost-to-go matrix. Then, the resulting cos-to-go matrix was indexed by the position in the route and is used on the real-time controller by applying the one-step look-ahead roll-out algorithm. Simulation results demonstrate the controller effectiveness in addressing ZEZ restrictions, presenting a trade-off between energy consumption and tailpipe NOx emissions. A benchmark was carried out, comparing the results obtained with the DP solution as the baseline, assuming perfect knowledge of driving cycle disturbances, revealing a 7% increase in tailpipe NOx emissions and a 1.3% increase in fuel consumption compared to the theoretical minimum and fulfilling the ZEZ restrictions in all the cases.

Keywords

Energy management strategy, hybrid electric vehicles, emissions control, vehicle emissions, look-ahead control

Introduction

Nations globally have established diverse policies to achieve carbon neutrality to mitigate environmental problems.[1] As of February 2021, 124 countries have committed to achieving carbon neutrality by 2050 or 2060.[2] To reach these targets, national governments and the European Union have implemented a range of initiatives, with one of the most widely adopted strategies being the promotion of electrified vehicles, which includes Battery Electric Vehicles (BEV) and Hybrid Electric Vehicles (HEV).[3] Another policy that has gained traction and expanded across major urban areas is the establishment of Low-Emission Zones (LEZ), or in the limit Zero-Emission Zones (ZEZ).[4,5] These zones impose stringent restrictions on pollutant emissions or, in some cases, implement outright bans, as seen in ZEZs where internal combustion engines are prohibited from operating within designated regions, so the use of conventional internal combustion engine vehicles is restricted in these areas.[6]

[1]CMT-Clean Mobility & Thermofluids, Universitat Politècnica de València, Valencia, Spain.
[2]Department of Engineering, University of Naples "Parthenope", Napoli, NA, Italy

Corresponding author:
Douglas Uberti Pinto, CMT-Clean Mobility & Thermofluids, Universitat Politècnica de València, Camino de Vera s/n, Valencia, 46022, Spain.
Email: dpdouube@mot.upv.es

In adherence to stringent emission regulations within ZEZs, only Battery Electric Vehicles (BEVs) or Plug-in Hybrid Electric Vehicles (PHEVs) operating in electric mode are allowed to access these regions.[7] While BEVs contend with limited driving range,[8] PHEVs offer versatility by seamlessly transitioning between electric, hybrid, or pure Internal Combustion Engine (ICE) modes, thereby accommodating diverse operating conditions.[9] This flexibility enables PHEVs to mitigate range constraints and sustain electric operation over prolonged periods.[10] However, to fully access the capabilities of HEVs, the effective management of the Energy Management System (EMS) is crucial. The EMS oversees the energy flow within the vehicle, with a focus on minimizing fuel consumption while satisfying driving power requirements. Additionally, it must address various constraints, including maximum power limits, and ensure that the battery State of Charge (SoC) remains within specified parameters.[11]

A PHEV can run in three main modes. The Charge-Depleting (CD) mode, which prioritizes electric mode driving until the battery SoC reaches a predetermined low level. The Charge-Sustaining (CS) mode, which operates in hybrid mode to maintain the SoC level and prevent deep discharges of the battery.[12] Alternatively, a blended operating mode can be utilized if the future driving conditions are known in advance. In this mode, both electric-only and hybrid modes are combined throughout the entire trip to guarantee overall energy consumption.[13,14]

The primary challenge of utilizing a PHEV within a ZEZ is ensuring sufficient battery energy to enter the area without engaging the engine, thereby operating in an electric-only mode in order to avoid engine use inside the forbidden area, then operate in CD mode.[15] Moreover, for PHEVs equipped with diesel ICE, the After-Treatment System (ATS) assumes critical importance in managing emissions. In this scenario, advanced EMS development is vital to accurately address real-world emissions impact, contrasting with standard homologation cycles.[16] Furthermore, when exiting the ZEZ, the ATS should be able to abate the emissions generated by the ICE and consider the light-off temperature to achieve tailpipe emissions abatement in such conditions.[17] This way, a robust and comprehensive control system becomes essential in HEV control by incorporating the ATS in the control strategies. Such a system must handle power distribution between the ICE and the electric motor to maintain the battery SoC at a desired level while overseeing the after-treatment system to minimize tailpipe emissions.[18]

The control strategies typically used in PHEV energy management involve rule-based strategies[19] and the Equivalent Consumption Minimization Strategy (ECMS) approaches.[20] These methods have the advantage of adaptability for real-time control applications. However, there is potential for improvement since their dependence on intensive calibration efforts or in calibrating the equivalency factor (ECMS) may not account for the variety of driving circumstances the vehicle might experience. Moreover, offline optimization methods like Pontryagin's Minimum Principle (PMP)[12] and Dynamic Programming (DP)[21,22] are often employed to devise optimal control strategies, extract near-optimal control patterns, or serve as benchmarks. Nonetheless, their dependence on perfect knowledge of driving cycle disturbances makes them unsuitable for real-time control applications.[23]

Concerning the development of control strategies for PHEV surrounding ZEZ, the widespread technique employed to address this problem is using adaptative ECMS-based approaches or developing strategies to calculate a SoC reference to enter the ZEZ with enough energy storage in the battery. For instance, Soldo et al.[10] combined a rule-based controller and an ECMS approach, generating an optimal SoC reference trajectory to enable the electric mode in the LEZ. Similarly, Capancioni et al.[24] exploits Vehicle-to-Network (V2N) communication to estimate future driving conditions and, with a dedicated algorithm, predicts the SoC value needed to cover the ZEZ to fulfill the trip in electric mode. An adaptive ECMS is also employed to reach the ZEZ limit with the SoC desired level.

In the case of PHEV urban buses or heavy-duty vehicles equipped with diesel engines, the design of the EMS must address fuel usage while ensuring emissions remain compliant with legal standards.[25] The efficiency of the after-treatment system used to reduce tailpipe emissions is significantly influenced by system temperature, such as during cold starts or warm-up periods.[26] These conditions present challenges for controlling PHEVs in the presence of ZEZ. Consequently, few studies have proposed strategies for managing PHEVs within ZEZ environments while considering the impact on tailpipe NOx emissions. For instance, Kupper et al.[27] proposed a self-learning energy management system for a PHEV, employing an adaptive supervisory controller with modular energy and emission management capabilities to address the constraints of maintaining sufficient battery energy while meeting real-world tailpipe NOx emissions requirements. The study findings underscore the critical nature of cold starts upon exiting the ZEZ. To address this issue,[17] developed a thermal management system to preheat the after-treatment system before entering a green zone, mitigating the impact of cold and inefficient after-treatment systems. The strategy employs two engine operation modes: one that prioritizes fuel efficiency and another that focuses on heat-up modes, heating the ATS less fuel-efficiently. However, this approach does not account for the broader impact of the strategy on the entire HEV powertrain.

The work described in this paper proposes a supervisory controller for energy management of an urban PHEV bus operating along a route with a ZEZ restriction. To account for the tailpipe NOx emissions and total energy consumption, the complete vehicle model integrates the powertrain system and the ATS. In this scenario, the supervisory controller is tasked with managing the power-split and controlling an electric heater added in the ATS to mitigate issues related to increased NOx emissions during daily vehicle operation, as well as during cold starts and warm-up periods, while achieving minimum fuel consumption. The strategy does not employ driving cycle prediction or adaptive ECMS to anticipate the SoC level target needed to travel in electric mode in ZEZ, as widely implemented in the literature.[15,24,28,29] The proposed solution employs a DP optimization of a given reference trip covered by the bus in the route at hand. Once the bus covers the same route frequently, the periodicity of the route is exploited by the cost-to-go matrix indexed by bus position and used as a control policy on the EMS of the future trips to be covered.

This paper is structured into six sections. Section "Case study and route analysis" outlines the case study scenario and provides an analysis of the bus route. Section "PHEV system description" offers a comprehensive description of the considered PHEV architecture and its unique features. The formulation of the optimal control problem and the operation of the supervisory controller are detailed in Section "Supervisory controller." Section "Results and discussion" presents the simulation campaign and discusses the obtained results. Finally, the conclusions are presented in Section "Conclusions."

Case study and route analysis

The study aims to propose supervisory energy management for a plug-in hybrid electric urban bus operating within the restriction of a ZEZ. The analysis focuses on the Line 72 urban route in Zurich, utilizing data sources from an open-access dataset.[30] This dataset encompasses several years of data collected from two trolley buses operating in Zurich across various routes, comprising over a thousand missions conducted in different seasons. The dataset includes detailed information on vehicle power demand, propulsion system, odometry, global positioning, ambient temperature, and other relevant parameters. Further information on the dataset and measurement methodology can be found in Scientific Data.[30]

Figure 1 shows the path of the selected bus line, a completed trip spans 18 km, with the bus initiating the journey at location A, reaching the destination B, and subsequently returning to A. To simulate the effect of a ZEZ, a restriction was added to this specific route, where the PHEV bus must operate in electric mode within the confines of its area. Consequently, the bus traverses the ZEZ twice (round trip), covering a total of 8 km exclusively in fully electric mode, during which the ICE must be switched off. The used data period contains measurements collected from June 22, 2019, to August 3, 2019, consisting of 108 complete trips. In addition to the speed profile derived from the dataset,

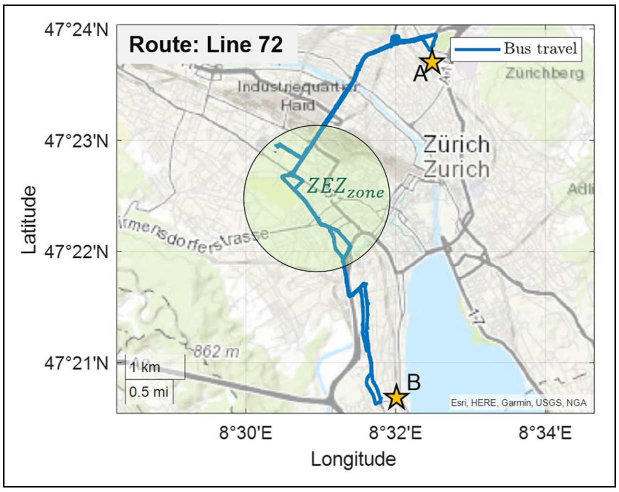

Figure 1. Bus odometry presents the bus position covering route 72 in Zurich, assuming the ZEZ restrictions on the percurse.

factors such as road slope, the total number of passengers, and ambient temperature are also considered as disturbances in modelling the problem.

As discussed in previous work,[31] urban bus routes may exhibit similarities across different journeys. These similarities stem from factors such as traversing the same path, passing through bus stops, encountering similar traffic lights and driving conditions, or to a predefined schedule between stops that drivers must adhere to. Figure 2 illustrates the speed profiles utilized, plotted over both spatial and temporal axes for the 108 available driving cycles. It is evident that each complete trip exhibits varying time durations. For instance, from trip 30 to 50, the bus frequently stops at the end of the outward trip, at destination B, then spends some time until the start of the return trip to A. However, when examining the speed profiles in the spatial domain, a stronger correlation between driving cycles becomes apparent. Therefore, the driving cycle study will focus on the speed profile data considering the bus distance inside the route instead of time.

An in-depth analysis of driving history data is crucial for two main reasons. Firstly, to verify the degree of similarity between driving cycles, determining how representative any individual driving cycle is compared to others. So, in this case, merely observing the velocity profiles in Figure 2 is insufficient to provide any conclusion. Secondly, it is important to investigate whether stronger correlations exist between consecutive trips, trips conducted at similar times, or trips on the same day, as the bus can be subject to similar driving conditions. For example, comparing peak traffic hours with late at night, the traffic conditions may be less congested for the second case, or even due to variations in passenger numbers resulting from people use of the public transport system. Therefore, identifying a driving cycle that is more representative of typical conditions could offer a valuable opportunity to develop a

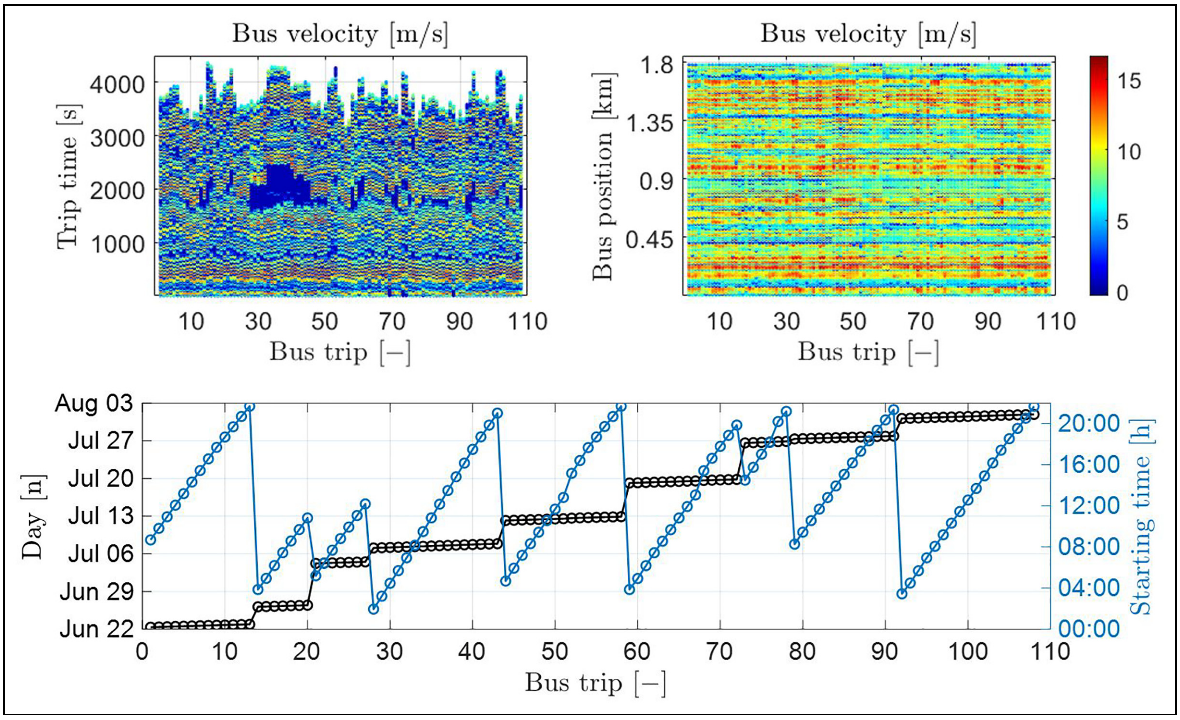

Figure 2. Upper plot: Bus velocity traces in time and distance domain for the 108 trips covered by the bus between June 22, 2019, and August 3, 2019. Bottom plot: Bus trip schedule organized by day and hour in ascending order.

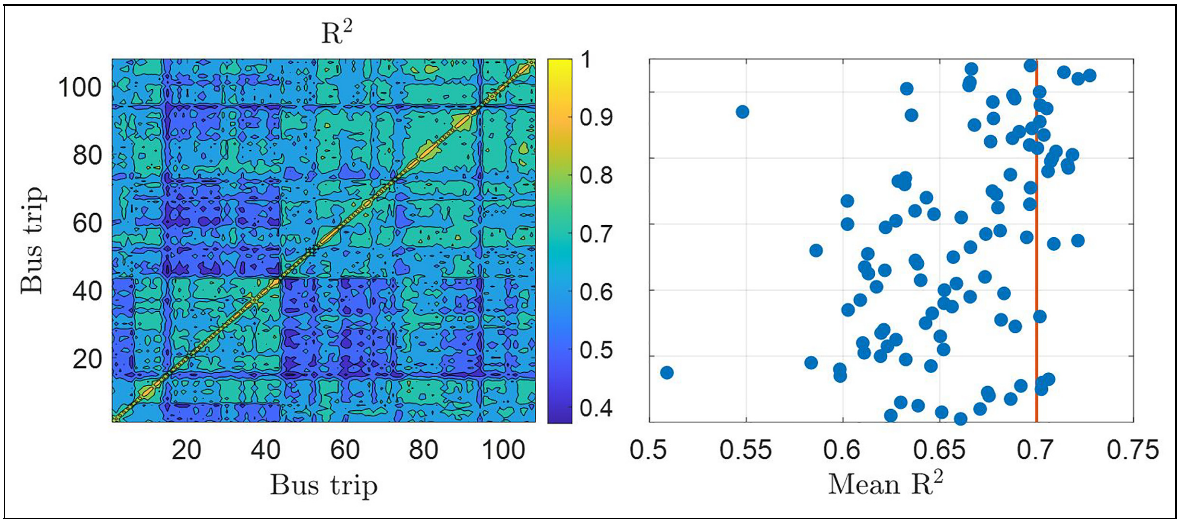

Figure 3. Representation of the correlation coefficients between the 108-vehicle-speed traces in distance.

control policy that enhances the energy management strategy for the bus.

To understand the similarities among various bus trips, computing the coefficient of determination, denoted as (R squared), between pairs of driving cycles can offer insights into their correspondence. The R^2 value is a statistical measure that indicates how well one set of data points (e.g., the speed profile of a trip) can be predicted by another. It ranges from 0 to 1, with higher values indicating a stronger correlation between the two datasets. Specifically, an R^2 of 1 indicates a perfect fit, while an R^2 close to 0 suggests little to no relationship between the compared trips. In the first step, the delays between pairs of driving cycles were identified to compensate for any measurement error that may occur during data collection, and then the speed traces were aligned. The contour plot on the left side of Figure 3 displays the R^2 values of the vehicle speed traces in space basis for the different driving cycles.

The minimum R^2 value observed in the contour plot on Figure 3 (left plot) among all bus trips is 0.4. At the same time, the maximum coefficient of 1 corresponds to instances where the comparison is within the same driving cycle (diagonal). Notably, the contour plot reveals two prominent regions with a higher correlation spanning trips. The first group spans from trip 13 to 43 and the second from 44 to 108. Within these regions, correlation coefficients generally range from 0.65 to 0.85, with occasional dips to 0.5 in the surroundings of these groups.

These results yield two significant conclusions. Firstly, individual speed traces from any trip within the dataset can reasonably estimate the bus velocity evolution, suggesting that past driving cycle data can be valuable for optimization tasks or control strategy development in HEVs. Secondly, despite variations in starting times, as shown in the bottom plot of Figure 2, similar trip patterns do not correlate with the journey commencement time within these regions. For instance, the two prominent regions span from starting times ranging from 00:00 to 20:00. Also, a higher correlation often occurs between two or three consecutive trips, as opposed to those separated by periods of four trips or more.

The right plot of Figure 3 compares the mean R^2 values, which reflect the correspondence between each trip and all others. The mean R^2 values for the trips range from 0.5 to 0.73, indicating varying degrees of similarity between trips. While no clear pattern was identified across all trips, those on the right side of the red curve exhibit higher correlations, higher than values of 0.7, which indicates that they may be more representative of the overall dataset. Furthermore, there are trips that mostly fall within the second group (44 to 108), which present a higher correlation with all the data sets. So, one can expect that selecting one of these speed traces as a reference for the selected route can capture, to some extent, the key particularities of the route.

Both the bus speed/distance trace plots and correlation analyses in the dataset demonstrate a close relationship between the speed profiles experienced by the bus during various trips. Consequently, utilizing one of the trips as reference data could provide valuable information for optimizing or developing new energy management strategies for future journeys along selected routes. Therefore, Section "Supervisory controller" will propose a supervisory energy management for controlling a PHEV exploiting the historical driving cycle data in the control policy of the EMS.

PHEV system description

This study was conducted in a simulation environment, and the PHEV model was constructed considering a P2 type parallel powertrain. This configuration was chosen to comply with the ZEZ restriction, taking into account the higher battery capacity required for electric driving mode. However, the proposed method can be adapted to address other architectures or scenarios.

PHEV model

Figure 4 depicts the PHEV system scheme, highlighting two main subsystems comprising the model. Firstly, the powertrain itself, where the power split needs to be controlled to meet the driver power demands while balancing energy consumption from two sources optimally. Secondly, the ATS plays a crucial role in PHEV configurations due to frequent bus stops, especially considering the ZEZ, where the ICE remains shut off for extended periods, reducing the ATS temperature and consequently decreasing SCR efficiency. To address this issue and study the impact of adding a heating device, an electric heater was integrated into the ATS. Both subsystems are integrated by the EMS embedded in the supervisory controller, which will be described in the next section. The impact of passenger numbers on the bus was also investigated to incorporate this factor into the route analysis. However, no discernible pattern was found in the route under consideration.

The approach employed in this paper to compute the optimal power distribution is based on the analysis of longitudinal vehicle dynamics, backward propagation, and the quasi-steady behavior of the ICE and the electric motor (EM). This method has been widely adopted in various studies focusing on the energy management system of HEVs. According to the hybrid architecture in Figure 4, the tractive power demand must be supplied by the ICE and the EM. They share the same speed due to the connection in the same shaft, so the relationship between the torque provided by the motor τ_{em} and the τ_{ice} defines as power split must be equal to the torque in the powertrain transmission τ_g.

$$\tau_g = \tau_{em} + \tau_{ice} \tag{1}$$

The transmission torque is obtained by discounting the transmission efficiency and η_g computing the final gear ratio of the selected gear g_r from the wheel to the main shaft:

$$\tau_g = \tau_w \, \eta_g \, g_r \tag{2}$$

The gear selection is outside the supervisory control, and a rule-based strategy is utilized to maintain the

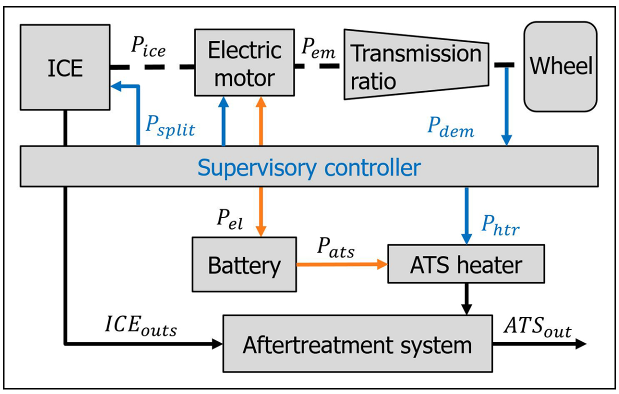

Figure 4. PHEV schematic overview.

engine and motor speeds within their optimal operating range. Similarly, the common couple rotational speed is computed by:

$$w_g = w_w \;\; g_r \tag{3}$$

Considering the input of the vehicle speed v and acceleration $\dot{v}$ and the disturbances provided by the bus dataset for a given bus trip, the torque at the wheels τ_w can be computed, so:

$$\tau_w = \left(m\,\bar{v}\,mg\mu cos\theta - mgsin\theta - \frac{11}{22}\rho A c_d v^2\right) r_w \tag{4}$$

where μ is the rolling coefficient, θ is road slope angle, ρ air density, Ac_d is the product of the bus frontal area and aerodynamic coefficient, r_w wheel radius. The number of passengers on the bus during the trajectories and the road slope are considered for the tractive demand computation. The total mass of the bus also accounts for the number of passengers, which is considered a mean mass of 70 kg per person.

The engine is represented by a static model, calibrated with experimental data and based on stationary maps. To develop these maps, a heavy-duty diesel engine was tested on a bench under steady-state conditions. The resulting maps predict several key output variables, including fuel mass flow $\dot{m}_f$, exhaust gas mass flow $\dot{m}_{exh}$, engine NOx emissions $\dot{m}_{NOx}$ and the exhaust gas temperature T_{exh} according to their inputs: τ_{ice} and w_g.

The EM was modelled using a quasi-static approach, where the map accounts for both positive and negative torques, where P_{em} represents its power consumption, which impacts the battery state of charge, discharging, or recharging it. A Thévenin equivalent circuit model was employed to capture the battery dynamics, depicting the battery as a resistor connected in series with a voltage source:

$$V = V_{oc} - I_b R_b \tag{5}$$

where R_b and V_{oc} are the battery internal resistance and the open circuit voltage based on the battery state of charge value SoC, respectively. The battery current I_b accounts for the electric energy involved in the tractive task and the electric power consumed by the electric heater P_{htr} added to the ATS, which will be described in the following subsection. Thus, the battery power is defined by:

$$P_b = P_{em} + P_{htr} \tag{6}$$

and the battery state of charge SoC will evolve as:

$$S\underline{o}C = -\frac{I_b}{C_b} \tag{7}$$

where C_b stands for the battery capacity. Once the torque in the powertrain transmission τ_g is defined based on the disturbance inputs, the τ_{em} and P_{htr} are the control variables that affect the SoC evolution.

After-treatment system model

The ATS thermal model was simplified as a single-order model, incorporating main components such as the Diesel Oxidation Catalyst (DOC) and Selective Catalytic Reduction (SCR) within the ATS. This simplification was necessary to facilitate DP computations, as the PHEV model already considers the SoC as a state variable. The decision to simplify was driven by the computational challenges associated with the curse of dimensionality, wherein increasing the discretization and number of system states and actuators demands significant computational resources to evaluate the combinations required for problem solution.

However, this approach still enables a meaningful comparison among different methodologies. The modelling approach follows that proposed in Donkers et al.[32], where the DOC and SCR are lumped in a single node whose temperature, denoted as after-treatment system temperature T_{ats}, representing both catalytic converters. This simplification involves calculating the total heat capacity of the entire system by summing the heat capacities of each individual component. As a result, the evolution of the ATS temperature is given by:

$$\dot{T}_{ats} = -\frac{c_{exh}}{C_{ats}}\dot{m}_{exh}(T_{exh} - T_{ats}) + \frac{h_{amb}}{C_{ats}}(T_{amb} - T_{ats}) + \eta_{htr}P_{htr} \tag{8}$$

where T_{ats}, T_{exh}, and T_{amb} represent the after-treatment system, engine-out gases, and ambient temperatures, respectively. The ATS model parameters c_{exh}, C_{ats}, and h_{amb} are specified in Table 1. The last term in the equation accounts for the power provided by the electric heater added to warm the ATS when it is switched on, and η_{htr} is the efficiency.

The SCR conversion efficiency η_{SCR} is a nonlinear function highly influenced by the temperature. This nonlinearity arises because the chemical reactions

Table 1. Description of the PHEV bus model main characteristics.

Bus model main features.	
Parameter name	**Value**
Weight	12000 kg
Frontal area	7.24 m^2
Drag coefficient	0.78
Motor rated power	180 kW
Battery capacity	78 kWh
Engine rated power	235 kW
Engine displaced volume	6.6 L
After-treatment model parameters.	
SCR volume	0.0163 m^3
ATS total heat capacity (C_{ats})	16500 J K^{-1}
Ambient heat transfer coefficient (h_{amb})	15 J K^{-1}s^{-1}
Specific heat capacity exhaust gas (c_{exh})	1100 J K^{-1}kg^{-1}

involved in reducing NOx emissions through SCR are highly temperature-dependent. At lower temperatures, typically below 200°C, the reduction reactions between ammonia (or urea) and NOx proceed too slowly, resulting in poor conversion efficiency. As the temperature increases, the reaction rate also increases, leading to significantly higher NOx conversion efficiencies. Given the simplification of the model, in line with the mapping used in D'Aniello et al.[33], simulations were conducted to map the efficiency based on T_{ats}, fixed pre-SCR concentration ratio C_{NO_2}/C_{NO_x} of 0.5 and space velocity SV. The latter is computed based on the ICE outputs (m_{exh} T_{exh} ρ_{exh}). Finally, the tailpipe NOx emissions can be estimated by:

$$NO_{x,tp} = NO_{x,exh} \ \eta_{SCR} \tag{9}$$

where $NO_{x,exh}$ is the engine out emission estimated by the stationary map. Similiar to PHEV model, the evolution of the after treatment system temperature (T_{ats}) is influenced by the control variables (τ_m and P_{htr}).

Supervisory controller

Optimal control problem

The proposed supervisory controller is designed to achieve the required energy and emission management for the PHEV while adhering to the ZEZ restrictions. It manages the battery state of charge and the after-treatment system temperate while minimizing fuel consumption and NOx tailpipe emissions by controlling the operating conditions of the engine and the electric heater. The control architecture is presented in Figure 4, and the details of the supervisory controller are discussed below. The following generic cost function represents the optimization problem:

$$J = \Phi\left(x\left(t_f\right)\right) + \int_{t_0}^{t_f} L(x(t), u(t), w(t))dt \tag{10}$$

where $\Phi\left(x\left(t_f\right)\right)$ is a terminal cost associated with the deviation from the initial energy stored in the battery, added to avoid battery energy depletion and L represents the instantaneous cost function, given by:

$$L = \lambda P_f + (1 - \lambda) NO_{x,tp} \tag{11}$$

where x, u, and w are vectors containing the system states, control actions, and disturbances that affect the system evolution, respectively. P_f represents the power of fuel consumed by the engine, and the parameter λ is a weight factor that balances the fuel consumption and tailpipe NOx emissions in the objective function. The variation of this parameter will be discussed in the results section. Finally, the mathematical representation of the corresponding optimal control problem can be defined as:

$$u^* = argmin_u \int_{t_0}^{t_f} L(\mathbf{x}, \mathbf{u}, \mathbf{w})dt \tag{12a}$$

subject to:

$$\underline{\mathrm{x}} = f(\mathbf{x}, \mathbf{u}, \mathbf{w}) \tag{12b}$$

$$\Phi = \sigma_{cost}\left(SoC_{t_f} - SoC_{t_0} - \delta_{SoC}\right)^2 \tag{12c}$$

$$P_{dem} = \begin{cases} P_{ice} + P_{em}, & ZEZ = 0 \\ P_{em}, & ZEZ = 1 \end{cases} \tag{12d}$$

The system dynamics (12b) corresponds to the battery state of charge and the after-treatment temperature with state vector:

$$\mathbf{x} = [\ SoC\ T_{ats}]^T \tag{13}$$

and the decision variables:

$$\mathbf{u} = [\tau_m \ \ P_{htr}]^T \tag{14}$$

Two constraints were incorporated to address the ZEZ problem discussed in this paper. First, the restriction (12c) defines the allowable limits for battery energy variation during a single bus trip, and the terminal cost σ_{cost} was adjusted to this aim. It was determined by the initial condition of the battery state of charge SoC_{t_0} for a given trip to be covered and the final condition in SoC_{t_f}. In this sense, an acceptable tolerance of $\delta_{SoC} = 0.06$ was established by considering that the bus would complete a sequence of 10 consecutive trips over a full workday, with the SoC ranging from 80% to 20%. Afterward, the bus will stop and recharge the battery to 80% capacity to begin the next workday.

This penalty constraint is necessary because, without it, the optimization would tend to deplete the battery during the initial trips, mainly operating in electric mode to avoid fuel consumption and NOx emissions from engine operation. Second, the restriction (12d) considers the vehicle position in the trip to identify when it is surrounding the ZEZ, so in this case, the vehicle cannot run in the hybrid mode (ICE + EM), only in electric mode.

Supervisory proposed strategy

The supervisory controller plays a crucial role in implementing the energy management strategy to address the optimal control problem presented in Section "Optimal control problem." It is the central decision-making component to maintain the SoC around the desired level by computing the optimal power-split and considering the impact on tailpipe NOx emissions by controlling the electric motor torque and heater power based on real-time operating conditions. To address the challenge of driving cycle dependence of DP in HEV control, the proposed strategy leverages data acquired from a previous trip undertaken by the vehicle along the route. This data serves as input for the optimal control problem during the initial offline phase, assuming periodicity between trips on the specific route. By solving a Dynamic Programming (DP) optimization for the known disturbances, the proposed approach leverages the full potential of this optimal control tool for online control purposes. DP is capable of providing a globally optimal solution for a discrete optimization problem.[34] In this case, the DP optimization is solved in discretized time:

$$\mathcal{J}^*(x,k) = min_u\{L(x,u) + \mathcal{J}^*(x,k+1)\} \tag{15}$$

The state x and control u spaces can be discretized, and the problem can be solved numerically. The process begins at the final time step ($k = n - 1$) and works backward. At this step, the cost-to-go is initialized as $\mathcal{J}^*(x,n) = \psi(x(n))$, where $\psi(x(n))$ is related to the terminal cost (12c) associated with the battery state of charge constraint. Moving backward through each time step, the cost-to-go is accumulated across all possible states. This backward accumulation continues until the initial time step $\mathcal{J}^*(x,1)$. So the optimal solution is stored in the optimal cost-to-go matrix, indexed by time step kk and the combination of states $\mathcal{J}^*(x,k)$. As demonstrated by the cycle analysis, the duration of each journey may vary, but the distance covered remains the same for all cycles. Therefore, the optimal matrix is indexed by the vehicle position $\mathcal{J}^*(x,s)$. Consider that exploring the optimal cost-to-go matrix allows estimating not only the optimal control policy from an initial state but also from any point in the (x,s) space, leveraging the benefits of the DP in online control applications.

It has been show in 2 that the different trips in the route are similar and present the same covered distance. Consider Bellman's principle of optimality, which DP exploits, states, "An optimal policy has the property that whatever the initial state and initial decisions are, the remaining decisions must constitute an optimal policy with regard to the state resulting from the first decisions".[35] Then, we can assume that for a given partial trajectory inside the DP, the solution of a given trip in the route is also optimal between its initial and final states. Taking into account that the driving cycle analysis shows a close correlation between the trips. A given optimal cost-to-go matrix of any trip represented by $\mathcal{J}^*(x,s)_{ref}$ can provide a good estimative from any state x to a position s in any of the trips that may be explored as a base policy to improve EMS of this vehicle in the route at hand.

The proposed approach of this paper is based on the idea of the previous paragraph, wherein the cost-to-go matrix obtained from offline optimization is integrated with the instantaneous cost function (11). To achieve this integration, the rollout algorithm[36] is employed. The controller depicted by the following equation can address the problem presented in (12):

$$u_k = argmin_u\left\{L(x_k, w_k, u) + \mathcal{J}^*(f_k(x_k,u), s_{k+1})_{ref}\right\} \tag{16}$$

where f_k represents the discrete version of the state function (12b), L stands for the instantaneous minimization of the cost function (11) or running cost and $\mathcal{J}^*(f_k(x_k,u), s_{k+1})_{ref}$ is an estimate of the optimal cost-to-go from the resulted state after applying the control u, obtained through interpolation within the reference solution $\mathcal{J}^*(x,s)_{ref}$.

With the basis of the preceding discussion and the analysis of the proposed rollout approach, the following conclusions can be outlined:

- The more the driving conditions and disturbances of the trip to be covered are similar to the reference trip ($\mathcal{J}^*(x,s)_{ref}$), the closer the solution will be to optimal.
- The algorithm can adjust its control policy based on feedback from the current system states, such as preventing battery SoC deviations out of the desired operating level.
- The proposed algorithm can integrate model predictive control (MPC) approaches by evaluating the sequence of L over a prediction horizon of length n. This is achieved by replacing the instantaneous cost in (16) with the cumulative cost over the selected horizon, which is represented by:

$$\int_{t_k}^{t_{k+n}} L(x_k, u_k, w_k)dt \tag{17}$$

Figure 5 displays the schematic representation of the proposed look-ahead control tailored for the specific case study presented on Section "Case study and route analysis." The bottom segment illustrates the offline component of the algorithm, which employs DP to solve a previously conducted bus trip along the same route. For this particular scenario, a singular trip that was previously recorded serves as the benchmark cycle. By utilizing DP, the cost-to-go of the reference trip is determined and subsequently stored in a map denoted as $\mathcal{J}^*\left(S\bar{o}C, \overline{T}_{ats}, \overline{s}\right)_{ref}$, providing insights into the minimum cost to complete the trip based on any states or bus position in the route s_k.

In parallel, the upper box and the supervisory controller optimization illustrate the algorithm that runs in real time. Employing the model described in Section "PHEV system description," the running cost L (11) is computed with the power of fuel consumed $P_{f,k}$ and the tailpipe NOx emissions $NO_{x,tp,k}$ at each time step k, based on the motor torque T_m and the heater power P_{htr}, providing estimation of the states and position in the next bus position in the route s_{k+1}.

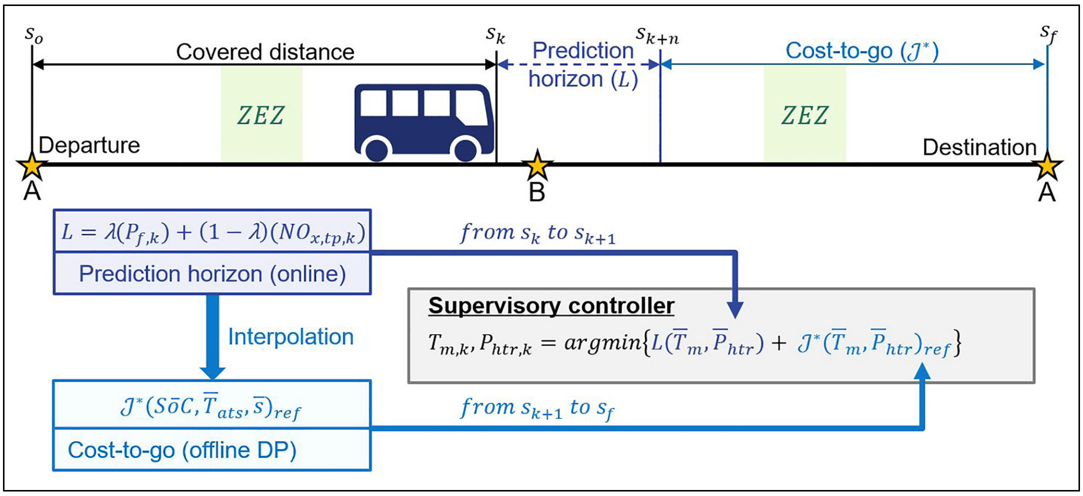

Figure 5. Block diagram of the proposed look-ahead algorithm applied in the case study of a PHEV covering an urban route subject to a zero-emission zone.

The predicted vehicle states within this prediction horizon are subsequently utilized to interpolate within the cost-to-go map, discerning the minimum cost from the s_{k+1} to the ending position of the route s_o. Subsequently, in the supervisory controller, the actions to be executed ($T_{m,k}$ and $P_{htr,k}$) are chosen to minimize not only the instantaneous cost but also the cumulative cost until the bus destination. Finally, the selected control actions are then applied to the PHEV system, updating the vehicle states, and the process is iteratively repeated throughout the entirety of the present trip until the trip's culmination.

Although this study focuses on an urban bus route in Zurich, the proposed energy management strategy is not limited to this specific case. The approach leverages the repetitive nature of urban bus operations, where routes are predictable and repeated daily. Allowing the use of past driving cycle data to perform offline optimizations, with the resulting cost-to-go matrix applied to real-time control. As such, the methodology can be generalized to any scenario where driving patterns exhibit periodicity, such as public transportation systems, delivery trucks, or other fleet operations that follow consistent routes, making the approach versatile and broadly applicable in scenarios with repetitive or predictable driving cycles.

Results and discussion

The performance assessment of the proposed supervisory controller involves comparing it with the Dynamic Programming solution, serving as the benchmark. In the DP solution, the complete bus trip speed profile and the disturbances are assumed to be known in advance, enabling the algorithm to compute optimal control trajectories. The evaluation scenario considers the PHEV completing ten consecutive bus trips within a complete working cycle. At the start, the SoC value is 0.8, and the EMS is tasked with managing the energy storage in the battery to adhere to ZEZ restrictions and achieve a minimum SoC close to 0.2 by the end of the duty cycle. This operational period spans approximately 12 h, with a stop of about 10 min after each trip. During this stop at the end of the trip, it is assumed that the ATS will reach the ambient temperature, simulating the impact of cold starting on each trip, and the SoC remains the same until the start of the next trip.

Figure 6 illustrates the evolution of states (T_{ats} and SoC) across the considered route over ten trips within a complete working day. The supervisory controller utilized the cost-to-go of a reference trip ($\mathcal{J}^*(x,s)_{ref}$) by selecting trip 101 from the complete dataset to conduct the DP optimization. Initially, for the DP calculations, the terminal cost (equation (10)) associated with battery state of charge deviations was tuned to maintain a difference close to 0.06 in the battery state of charge between the end and beginning of an arbitrary trip. Once this parameter was tuned, it remained constant throughout the simulation campaign. However, due to the length of a complete working day comprising ten trips, obtaining a DP solution for the entire day is infeasible due to computational limitations. Therefore, the DP solution has been applied for each trip, employing the tuned terminal cost for each trip. Providing a cumulative effect over the ten trips, leading to a global battery decay from 0.8 to 0.2 from the beginning to the end of the set of trips.

The complete trip results depicted in the upper plot of Figure 6 reveal a clear pattern across the successive journeys. Initially, the ICE charges the battery from the onset of each trip until reaching the ZEZ. Then, when exiting the ZEZ, the battery is recharged again, and as the ICE operates, the ATS temperature rises. This pattern persists throughout all the trips of the set, with the battery reaching its minimum value close to 0.2 by the end of the completed day. Since the supervisory controller is supplied with the cost-to-go of a reference trip

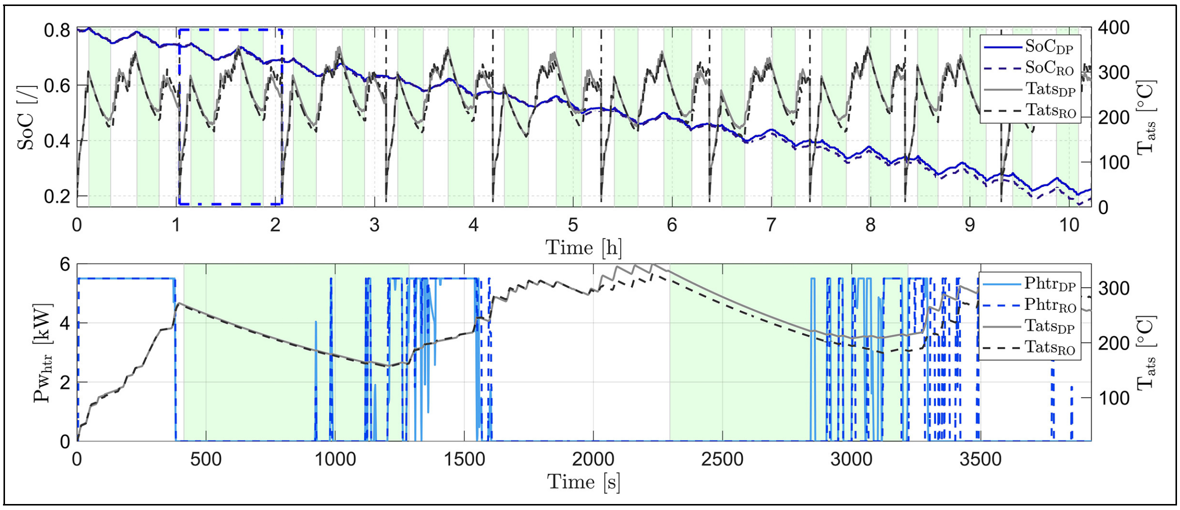

Figure 6. Representation of the complete route evaluated with the proposed supervisory controller and the DP presenting the SoC and ATS temperature evolution (upper). Depict of a single trip for the $\lambda = 0.2$ condition showing the impact of the heater power in the ATS temperature (bottom).

solved by DP, the state evolutions of both strategies remain similar. This observed pattern corroborates the findings outlined in the driving cycle analysis presented in this paper, highlighting the significant correlation across the various cycles analysed within the studied route.

When examining a specific trip, the lower plot of Figure 6 illustrates the heater power consumption and the ATS temperature evolution during the second trip within this sequence of covered trips in work daily. The parameter λ (equation (11)) balances the cost between fuel consumption and tailpipe NOx emissions. In this instance, λ is set to 0.2, prioritizing the minimization of tailpipe NOx emissions. With this configuration, it is observed that at the start of the trip, both strategies activate the heater to raise the ATS temperature quickly and achieve higher SCR efficiencies. Subsequently, as the bus enters the ZEZ, the temperature decreases while the ICE remains inactive. Upon exiting the ZEZ, the electric heater is activated again to elevate the ATS temperature before the ICE starts, and this process repeats during the return trip when the bus re-enters the ICE restricted zone. Note that some oscillations can be observed in the activation and deactivation of the heater, considering an additional state to penalize heater power variations could mitigate this problem. However, this aspect was neglected due to the computational cost requirements.

The upper plot in Figure 7 illustrates the relative electric heater energy consumption of the across different λ values, using the DP case with $\lambda = 0.2$ as a reference. This case imposes a high cost on NOx tailpipe emissions in the objective function (11), leading to the highest mean ATS temperature. As shown in the bottom plot, the temperature in this case is approximately 30°C higher than in cases with higher λ values (0.6 and 0.8), which do not activate the electric heater as it

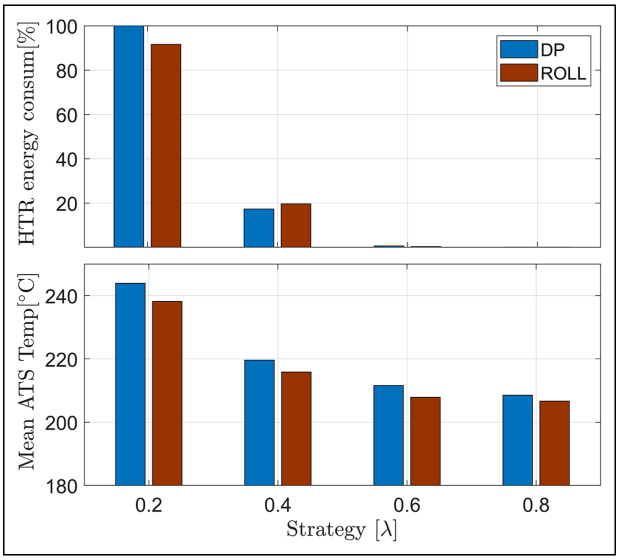

Figure 7. Relative heater energy consumption of proposed supervisory controller (ROLL) varying the value of λ compared to the DP case with $\lambda = 0.2$ and mean ATS temperature evaluated in consecutive 100 trips.

minimizes energy consumption. In the $\lambda = 0.4$ case, although 20% of the heater's energy is utilized, the resulting ATS temperature is still around 20°C lower. Across all λ values, the energy consumption and ATS temperatures observed with the RO controller follow similar trends to those of the DP solution. It is important to note that the ATS temperature is also influenced by the composition of the engine exhaust gases, meaning that the results are further affected by the operating conditions of the engine.

Figure 8 illustrates the frequency of engine operating conditions obtained with both the DP and supervisory algorithm across various λ values. For lower values of

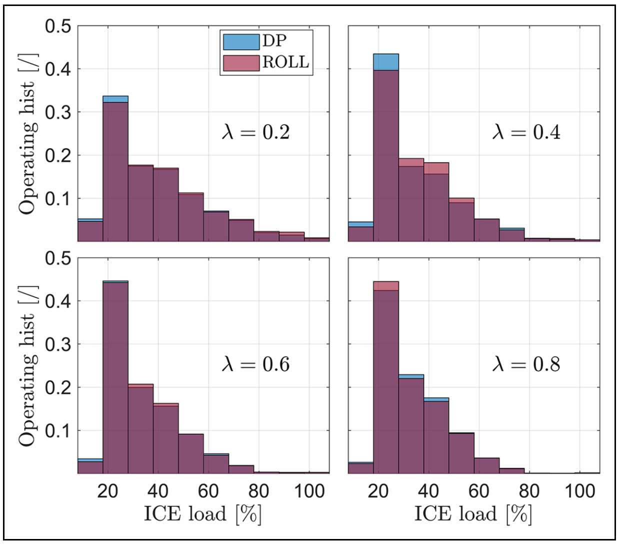

Figure 8. Comparison between the engine operating point histogram obtained with DP assuming the perfect knowledge of the route (optimal solution) with the proposed online applicable method (ROLL) for the four values of λ evaluated in 100 consecutive trips.

λ, it was observed that the ICE operating conditions are distributed evenly along the range, occasionally reaching 100% of engine load. Conversely, for higher values, the distribution tends to concentrate around lower loads, with a maximum of 70% of engine load. A higher engine load can also assist in maintaining a higher ATS temperature, as the exhaust mass flow and the temperature of engine exhaust gases increase, as indicated in equation (8). However, it can penalize fuel consumption once the ICE works in lower-efficiency regions. In the same way that the supervisory controller strategy leads to a similar evolution of SoC and ATS temperature as DP results, the ICE operating conditions distribution also approaches the DP solution for all λ values evaluated, showing the potential of the proposed approach.

In summary, the trade-off for four values of λ, as depicted in Figure 9, illustrates that the supervisory controller can achieve results comparable to DP optimization, which relies on perfect foreknowledge of driving cycles and disturbances. This study aims to demonstrate the impact of selecting a random trip route for control purposes. Each journey in the dataset was evaluated in DP optimization to construct the cost-to-go matrix and subsequently utilized in the control policy to oversee the bus throughout the entire route (100 driving cycles). The scatter plot depicts the results obtained by the proposed supervisory controller when evaluating the 100 reference trips, and the colorbar represents the mean R^2 value obtained by the driving cycle analysis presented in Section "Case study and route analysis." Meanwhile, the percentages represent the mean and standard deviation of penalties relative to the results obtained by DP optimization.

The mean penalty concerning the DP results ranges from 1.25% to 1.5% when considering fuel consumption across all values of λ. Conversely, higher penalties are observed for mean tailpipe NOx emissions ranging from 2.3% to 7%. Despite the increased penalty for NOx tailpipe emissions at $\lambda = 0.2$, which prioritizes emissions reduction, it is noteworthy that the supervisory controller effectively maintains emissions close to low levels, close to 0.1 g/kWh. In this same scenario, there is a particular case where the rollout

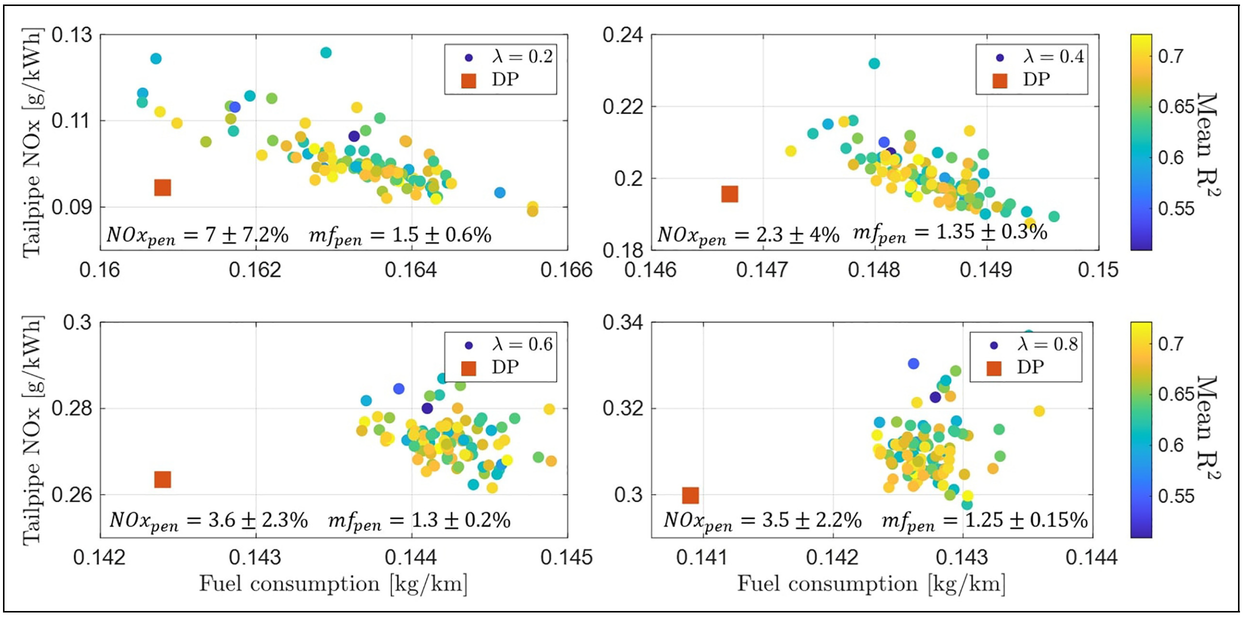

Figure 9. Summary of supervisory controller performance calibrated with all trips for the four values of λ and then applied to the complete route dataset. The percentages represent the mean and standard deviation of penalties relative to the results obtained by DP optimization.

outperformed the results obtained by the optimal solution, providing a reduction of 0.2%. However, this occurs at the expense of increasing fuel consumption by 3%.

The results presented in Figure 9 further support the conclusions drawn from the driving cycle analysis. The concept under discussion suggests that if a driving cycle can be identified as more representative of the entire dataset and used as the reference trip for DP optimization, the resulting cost-to-go matrix may yield better performance than calibrations based on a randomly selected or less representative driving cycle. However, as seen in the dispersion plot, no significant performance improvement was observed when using trips with higher correlation for this application, and no clear trend emerged to confirm this hypothesis. This lack of improvement may be attributed to the nature of the multi-objective function employed by the controller, which seeks to balance two interdependent variables, fuel consumption and NOx emissions, both intrinsically linked to engine operation. On the other hand, when analysing the top ten results that achieved near-optimal performance in minimizing either fuel consumption ($\lambda = 0.8$) or tailpipe NOx emissions ($\lambda = 0.2$), it is notable that 50% of the corresponding R^2 values fall within the range of 0.7 to 0.75.

Conclusions

This paper presents a supervisory controller designed for PHEVs operating on daily routes. The strategy can manage ZEZ restrictions by ensuring full-electric driving and mitigating NOx tailpipe emissions, analyzing the trade-off at the expense of increasing fuel consumption. This is achieved using a cost-to-go matrix indexed by the vehicle position along a trip within the route generated by the DP optimization of a previous trip. From the numerical study, the paper main contributions can be summarized as follows:

- It has been demonstrated that when dealing with commuting regular trips such as urban bus routes, the past driving cycle data can be useful information for modelling control strategies in HEV.
- For the studied route, the driving cycle analysis shows that no patterns were found according to the daytime of trips or the number of passengers on the bus.
- The proposed supervisory EMS does not use a driving cycle prediction approach, but it discusses that the controller can be enhanced by combining such strategies with Model Predictive Control.
- Other system parameters can be addressed in this strategy but can strongly increase computational efforts due to dynamic programming optimization.
- An optimization criterion was discussed to address the trade-off between fuel consumption and NOx tailpipe emissions, enabling the customization of the value of λ to suit specific applications.

Funding

The author(s) disclosed receipt of the following financial support for the research, authorship, and/or publication of this article: This research has been partially funded by the Agencia Estatal de Investigación of Spain through the project PID2020-119691RB-I00, entitled ''Mantenimiento Y Control Optimo De Vehiculos Hibridos De Transporte Urbano Mediante Datos Del Contexto Operacional''.

References

1. Chen JM. Carbon neutrality: toward a sustainable future. *Innovation* 2021; 28: 2(3).
2. Chen L, Msigwa G, Yang M, et al. Strategies to achieve a carbon neutral society: a review. *Environ Chem Lett* 2022; 20(4): 2277–2310.
3. Ahmadi P. Environmental impacts and behavioral drivers of deep decarbonization for transportation through electric vehicles. *J Clean Prod* 2019; 225: 1209–1219.
4. Transport for London | Every Journey Matters. *Congestion Charge (Official)*. Available online: https://tfl.gov.uk/modes/driving/congestion-charge?cid = pp020 (accessed 01-03-2024).
5. Tesanovic M and Vadgama S. *Short paper: Vehicle emission control in Smart Cities*. In: *2014 IEEE World Forum on Internet of Things (WF-IoT)*, pp. 163–164, IEEE, 2014.
6. Oxfordshire County Council. *Oxford zero emission zone (ZEZ)*. Available online: https://www.oxfordshire.gov.uk/residents/roads-and-transport/oxford-zero-emission-zone-zez (accessed 01-03-2024).
7. Biswas D, Ghosh S, Sengupta S, et al. A Predictive supervisory controller for an HEV operating in a zero emission zone. In *2019 IEEE transportation electrification conference and expo (ITEC)*2019 Jun 19 (pp. 1–6). IEEE.
8. Xu F, Tsunogawa H, Kako J, et al. Real-time energy optimization of HEVs under-connected environment: a benchmark problem and receding horizon-based solution. *Cont Theory Technol* 2022; 20(2): 145–160.
9. Fantin Irudaya Raj E and Appadurai M. The hybrid electric vehicle (HEV)—an overview. *Emerg Sol e-Mobility Smart Grid Sel Proceed ICRES* 2020. 2021; 8: 25–36.
10. Faghih SE, Chitsaz I and Ghasemi A. A component sizing prediction study for a series hybrid electric vehicle

based on artificial neural network. *Int J Engine Res* 2024; 25(1): 47–64.
11. Soldo J, Skugor B and Deur J. *Optimal energy management control of a parallel plug-in hybrid electric vehicle in the presence of low emission zones*. SAE Technical Paper; 2019.
12. Padmarajan BV, McGordon A and Jennings PA. Blended rule-based energy management for PHEV: System structure and strategy. *IEEE Transact Veh Technol* 2015; 65(10): 8757–8762.
13. Han S and Ahn C. *Optimal preemptive controller enabling electric driving of a hybrid electric vehicle in a zero emission zone*. IEEE Transactions on Vehicular Technology. 2023 Nov 29.
14. Barbier A, Salavert JM, Palau CE, et al. Predicting instantaneous engine-out NOx emissions in a real-driving vehicle data scenario. *Int J Engine Res* 2023; 24(8): 3626–3641.
15. Climent H, Pla B, Bares P, et al. Exploiting driving history for optimising the energy management in plug-in hybrid electric vehicles. *Energy Conv Manag* 2021 Apr 15;234:113919.
16. Bellman RE and Dreyfus SE. *Applied dynamic programming*. Princeton University Press; 2015.
17. Onori S, Serrao L and Rizzoni G. *Hybrid electric vehicles: Energy management strategies*. London, UK: Springer; 2016.
18. Yu H, Kuang M and McGee R. Trip-oriented energy management control strategy for plug-in hybrid electric vehicles. *IEEE Transact Veh Technol* 2013; 22(4): 1323–1336.
19. Zhang F, Hu X, Langari R, et al. Energy management strategies of connected HEVs and PHEVs: Recent progress and outlook. *Prog Energy Combust Sci* 2019; 73: 235–256.
20. Holmer O, Willems F, Blomgren F, et al. *Optimal aftertreatment pre-heat strategy for minimum tailpipe NO x around green zones*. SAE Technical Paper; 2020 Apr 14.
21. Peng J, He H and Xiong R. Rule based energy management strategy for a series–parallel plug-in hybrid electric bus optimized by dynamic programming. *Appl Energy* 2017; 185: 1633–643.
22. Bellman R. Dynamic programming. *Science* 1966; 153(3731): 34–37.
23. Zhu D, Pritchard E, Dadam SR, et al. Optimization of rule-based energy management strategies for hybrid vehicles using dynamic programming. arXiv preprint arXiv:2207.06450. 2022 Jul 8.
24. Kong Y, Xu N, Liu Q, et al. A data-driven energy management method for parallel PHEVs based on action dependent heuristic dynamic programming (ADHDP) model. *Energy* 2023; 265: 126306.
25. Lewis FL, Vrabie D and Syrmos VL. *Optimal control*. John Wiley & Sons; 2012.
26. Bertsekas D. Rollout algorithms for constrained dynamic programming. *Lab Inform Decision Sys Report* 2005; 2646: 45–50.
27. Capancioni A, Brunelli L, Cavina N, et al. *Development of adaptive-ECMS and predictive functions for Plug-in HEVs to handle Zero-Emission Zones using navigation data*. SAE Technical Paper; 2021 Sep 5.
28. Grahn M, Johansson K and McKelvey T. Data-driven emission model structures for diesel engine management system development. *Int J Engine Res* 2014; 15(8): 906–917.
29. D'Aniello F, Arsie I, Pianese C, et al. Development of an Integrated Control Strategy for engine and SCR system basedon effective EGR rate. *IFAC-PapersOnLine* 2020; 53(2): 14034–14039.
30. Wooldridge MS, Singh R, Gutierrez LG, et al. Survey of strategies to reduce cold-start particulate, CO, NOx, and hydrocarbon emissions from direct-injection spark-ignition engines. *Int J Engine Res* 2023; 24(2): 456–480.
31. Kupper F, Mentink PR, Meima N, et al. *Towards self-learning energy management for optimal phev operation around zero emission zones*. SAE Technical Papers. 2022 Mar 29;2022.
32. Brunelli L, Capancioni A, Canè S, et al. A predictive control strategy based on A-ECMS to handle Zero-Emission Zones: performance assessment and testing using an HiL equipped with vehicular connectivity. *Appl Energy* 2023; 340: 121008.
33. Polverino P, Arsie I and Pianese C. Optimal energy management for hybrid electric vehicles based on dynamic programming and receding horizon. *Energies* 2021; 14(12): 3502.
34. Scientific Data. *ZTBus: A large dataset of time-resolved city bus driving missions*. Available online: https://www.nature.com/articles/s41597-023-02600-6 (accessed 05-03-2024).
35. Tormos B, Pla B, Bares P, et al. Energy management of hybrid electric urban bus by off-line dynamic programming optimization and one-step look-ahead rollout. *Appl Sci* 28; 12(9): 4474.
36. Donkers MC, Van Schijndel J, Heemels WP, et al. Optimal control for integrated emission management in diesel engines. *Control Eng Pract* 2017; 61: 206–216.